A New Method for Estimation of Velocity Vectors

Jørgen Arendt Jensen, *Member, IEEE*, and Peter Munk

***Abstract*—The paper describes a new method[1] for determining the velocity vector of a remotely sensed object using either sound or electromagnetic radiation. The movement of the object is determined from a field with spatial oscillations in both the axial direction of the transducer and in one or two directions transverse to the axial direction. By using a number of pulse emissions, the inter-pulse movement can be estimated and the velocity found from the estimated movement and the time between pulses. The method is based on the principle of using transverse spatial modulation for making the received signal influenced by transverse motion. Such a transverse modulation can be generated by using apodization on individual transducer array elements together with a special focusing scheme. A method for making such a field is presented along with a suitable two-dimensional velocity estimator. An implementation usable in medical ultrasound is described, and simulated results are presented. Simulation results for a flow of 1 m/s in a tube rotated in the image plane at specific angles (0, 15, 35, 55, 75, and 90 degrees) are made and characterized by the estimated mean value, estimated angle, and the standard deviation in the lateral and longitudinal direction. The average performance of the estimates for all angles is: mean velocity 0.99 m/s, longitudinal S.D. 0.015 m/s, and lateral S.D. 0.196 m/s. For flow parallel to the transducer the results are: mean velocity 0.95 m/s, angle 0.1°, longitudinal S.D. 0.020 m/s, and lateral S.D. 0.172 m/s.**

I. Introduction

It is a common problem to measure the velocity of a moving object, when the object is observed with a probing field. Equipment of this kind is used in medical ultrasound to measure the velocity of blood flow noninvasively. Here an ultrasound beam is emitted by a transducer. The ultrasound field then interacts with the blood and gives rise to a scattered field, which is received by the transducer. Emitting a second pulse then yields a received signal that is displaced in time compared to the first signal, due to the movement of the blood between pulse emissions. Repeating this a number of times yields signals suitable for velocity estimation. Sampling the received response at a fixed time after each pulse emission, corresponding to a fixed depth in tissue, results in an audio signal, with an audio frequency proportional to both the blood velocity along the ultrasound beam [1] and the emitted puls' RF frequency. This was used by Baker [2] to devise a system for displaying the velocity distribution at the depth of sampling. A Fourier transform of the sampled signal will yield the distribution as frequency is proportional to velocity. This technique also can be used to display velocity images by estimating the mean velocity at a particular depth, as described by Kasai *et al.* [3]. Here the ultrasound beam is emitted a number of times in one distinct direction, and the velocities along that direction are found by sampling the received signal for a number of depths and then estimate the mean velocities for the corresponding depths. The beam direction is then changed. The measurement procedure is repeated, and the velocities are found along the other directions. An image of velocity is then made, and continuously updated over time. The velocity can be found through an autocorrelation approach, as described by Kasai *et al.* [3] and Namekawa *et al.* [4]. Another technique is to use cross-correlation as described by Dotti *et al.* [5] and Bonnefous *et al.* [6]. A general description of ultrasound velocity estimation systems can be found in [1].

Radar systems also use the pulse-echo principle for estimating velocity of a moving object. A series of radar pulses is emitted, and the received signals are recorded. The signals from a specific distance are compared, and the velocity is calculated from the movement of the object between pulses, the speed of light, and the time between pulse emissions. This is, for example, used for finding the velocity of airplanes, missiles, or ships, described by Skolnik [7].

The pulse movement principle has also been employed in sonar for finding the velocity of different objects. This is done by the same methods as mentioned above for medical ultrasound scanners with appropriate adaptations.

A major problem with these velocity estimation techniques is that only the velocity component in the beam direction, i.e., toward or away from the transducer, can be found. Velocity components perpendicular to the beam propagation direction cannot be measured. A number of approaches have sought to remedy this in diagnostic medical ultrasound. Two consecutive ultrasound images are measured in the speckle tracking approach as described by Trahey *et al.* [8]. The movement of a regional pattern from one image to the next is found through two-dimensional cross-correlation, and the velocity vector for the region is determined from the displacement of the region and the time between the images. The technique needs two images, which makes data acquisition slow, and precludes the use of averaging. The image acquisition also makes this technique difficult to use for full three-dimensional velocity es-

Manuscript received October 6, 1997; accepted January 7, 1998. This work has been supported by B-K Medical A/S, Gentofte, Denmark and by grant EF 632 from the Academy of Technical Sciences of Denmark.

The authors are with the Department of Information Technology, Technical University of Denmark, DK-2800 Lyngby, Denmark (e-mail: jaj@it.dtu.dk).

[1]A patent is pending on the method described in this paper.

timation. The two-dimensional correlation necessitates a high number of calculations, and erroneous velocities can evolve due to false maxima in the correlation function [9].

Another approach is to use two transducers or apertures emitting two beams crossing each other in the region of interest, whereby the velocity can be found in two independent directions [10]. The velocity vector can then be found through a triangulation scheme. The variance, and hence the accuracy, of the transverse component of the velocity is affected by the angle between the two beams. The small angle between beams at large depths in tissue results in a high measurement variance, i.e., a low precision. The use of two transducers or a single large array also makes probing between the ribs of a person difficult and can result in loss of contact for one of the transducers.

Other techniques like beam-to-beam correlation [11] and changes in signal bandwidth [12] have been suggested. None of these techniques have, however, attained a performance that warrants commercial implementation.

The paper proceeds along the following lines: Section II introduces a new method for vector velocity estimation based on the observations from the introduction. The method uses a special probing field, and how to produce such a field is detailed in Section III. A suitable estimation algorithm for finding the vector velocity is described in Section IV, and a simulation of the performance is given in Section V.

II. A New Method for Estimation of Vector Velocity

The current systems estimate the velocity from the correlation between consecutively received signals. This is possible because the received signals have an oscillatory nature, which makes it possible to perform the phase-shift estimation of the autocorrelation approach or the time-shift estimation of the cross-correlation approach. The phase shift estimation is particularly efficient because it only needs one complex set of samples for each pulse-echo line to find the velocity magnitude and sign. Very few calculations (seven per sample) are needed for the estimation of the velocity [1]. The measurement of this set of samples can be done directly on the radio frequency data by just taking a sample at the depth of interest for the in-phase signal and a second sample $1/(4f_0)$ seconds later for the quadrature signal [1], [13]. Here f_0 is the center frequency of the emitted pulse. Velocity estimation is, thus, possible from the in-phase and quadrature samples, when they emanate from a signal with oscillations in the direction of the velocity component.

These two observations make it, in principle, possible to devise a measurement set-up for finding the velocity vector. A probing field is generated with oscillations in each direction for which the velocity component is of interest. Measurements of the in-phase and quadrature signals are then made for each pulse emission. These measurements are then used by an estimator to yield the velocity components in the preferred directions, thereby obtaining the velocity vector [14].

An illustration of the signal generation in a traditional velocity estimation system is shown in Fig. 1. An 8 cycle, $f_0 = 3$ MHz pulse is used for emission, and Gaussian apodization of the transducer and delay focusing are used during transmission and reception for generating the field. A snapshot of the received voltage at a fixed time is shown in the upper left graph. The graph shows the voltage received from the transducer, when a single scatterer is at the position indicated in the graph at the time of the snapshot. Dark areas correspond to negative voltages and light areas to positive voltages. Gray corresponds to zero. Thus, it is a depiction of the voltage that will result from sampling at the time of the snapshot. A moving scatterer will traverse the field and give rise to a sampled signal that is a function of the spatial field, the sampling time, and the scatterer's velocity. The dark lines indicate the voltage when traversing the field in the axial or the lateral direction. A purely axial velocity gives rise to a received signal that oscillates. If the time between pulses is T_{prf} and the scatterer's axial velocity is v_z, then the movement between pulses is $T_{prf}v_z$. At the center position this will result in a sampled signal as shown in Fig. 2. Here the frequency of the received signal is:

$$f_z = \frac{v_z}{\lambda/2} = \frac{2v_z}{c} f_0 \tag{1}$$

where $\lambda = c/f_0$ is the wavelength of the emitted pulse, and c is the speed of sound. Note that it is a pulse-*echo* measurement, hence $\lambda/2$ is used in (1). The frequency is:

$$f_z = \frac{|\vec{v}|\cos\theta}{\lambda/2} = \frac{2|\vec{v}|\cos\theta}{c} f_0 \tag{2}$$

if the velocity is at an angle θ with respect to the direction of the propagating ultrasound field. This also will introduce a modulation of the received signal from the lateral response of the field. For a purely transverse motion ($\theta = \pi$), a signal equal to the lateral response shown in the top right graph of Fig. 1 will be received, and no velocity can be detected because the frequency spectrum of the sampled signal is centered around zero frequency.

In order to make the sampled signal influenced by transverse motion, a lateral modulation of the field must be introduced. This is shown in Fig. 3 for an ideal field with an 8-cycle axial oscillation and a 4-cycle lateral modulation. The received voltage at a fixed time as a function of spatial position is shown along with the axial and lateral response as a function of different scatterer positions. The sampled response for a purely lateral movement is also shown in graph in Fig. 4(d). It can be seen how the signal is affected by the lateral movement, and it can, thus, be used for velocity estimation. The frequency for this signal is:

$$f_x = \frac{v_x}{d_x} \tag{3}$$

where d_x is the periodic distance of the lateral modulation and v_x is the lateral velocity. The received sampled signal is now affected by both axial and lateral movements

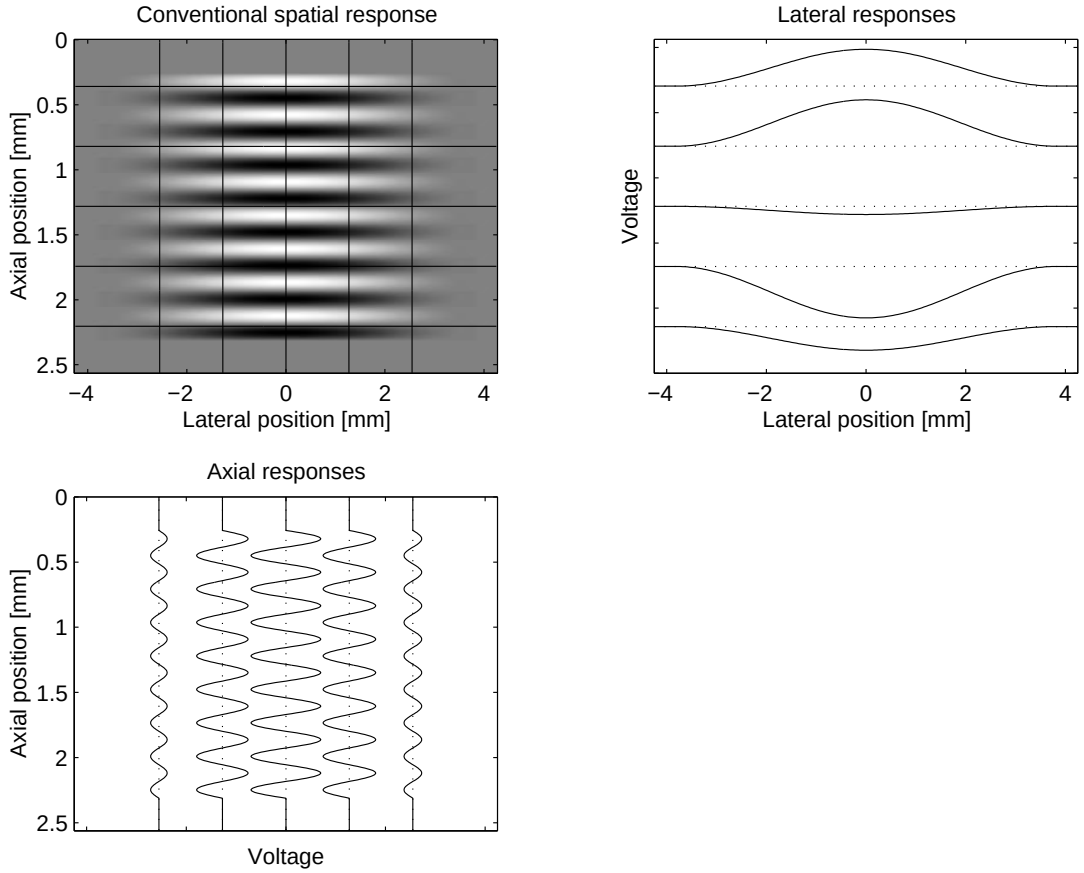

Fig. 1. Ideal received voltage from a single scatterer as a function of spatial position for a traditional ultrasound system.

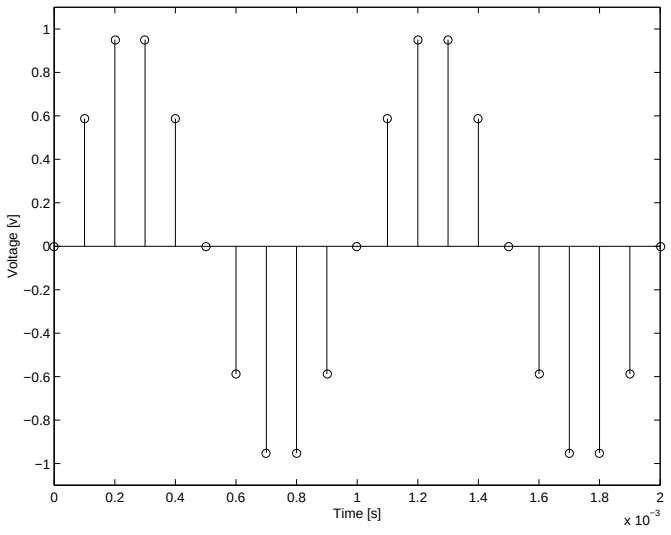

Fig. 2. Received voltage from a single scatterer traversing the field in the axial direction. The velocity v_z is 0.25 m/s, T_{prf} is 100 μs, and the transducer center frequency f_0 is 3 MHz.

as shown in Fig. 4 for different velocity directions. This demonstrates how the lateral modulation of the field results in a modulation of the received sampled signal, which then contains information about both axial and lateral velocity.

As mentioned in the introduction, the in-phase and quadrature signals must be measured to find the sign of the velocity. Four measurements then are needed in the new approach for finding the direction and magnitude of the velocity vector. Thus, it is necessary to employ a spatial quadrature sampling in which the two measurements give the in-phase and quadrature samples for the lateral direction. This can be done by having two probing fields in which the lateral modulation of the quadrature field is 90° phase-shifted compared to the in-phase field's lateral modulation. This is generated by having one emit beamformer and two receive beamformers working in parallel. Samples are acquired from the two received signals at time $2d_0/c$ and $2d_0/c + 1/(4f_0)$ to obtain the four measurements for both time and spatial quadrature sampling. These samples are then fed into the estimator to yield the velocity components.

Another processing option is to make a compensation for the axial velocity before determining the lateral velocity. The received lateral signals are affected by the movement in the axial direction of the beam. The velocity in the direction of the beam, therefore, is determined first, and the effect of the axial movement is compensated for in the received lateral signal, so that only transverse movement gives rise to a variation in the compensated signal. Standard techniques then can be used for finding the velocity or the velocity distribution, as used in a conventional

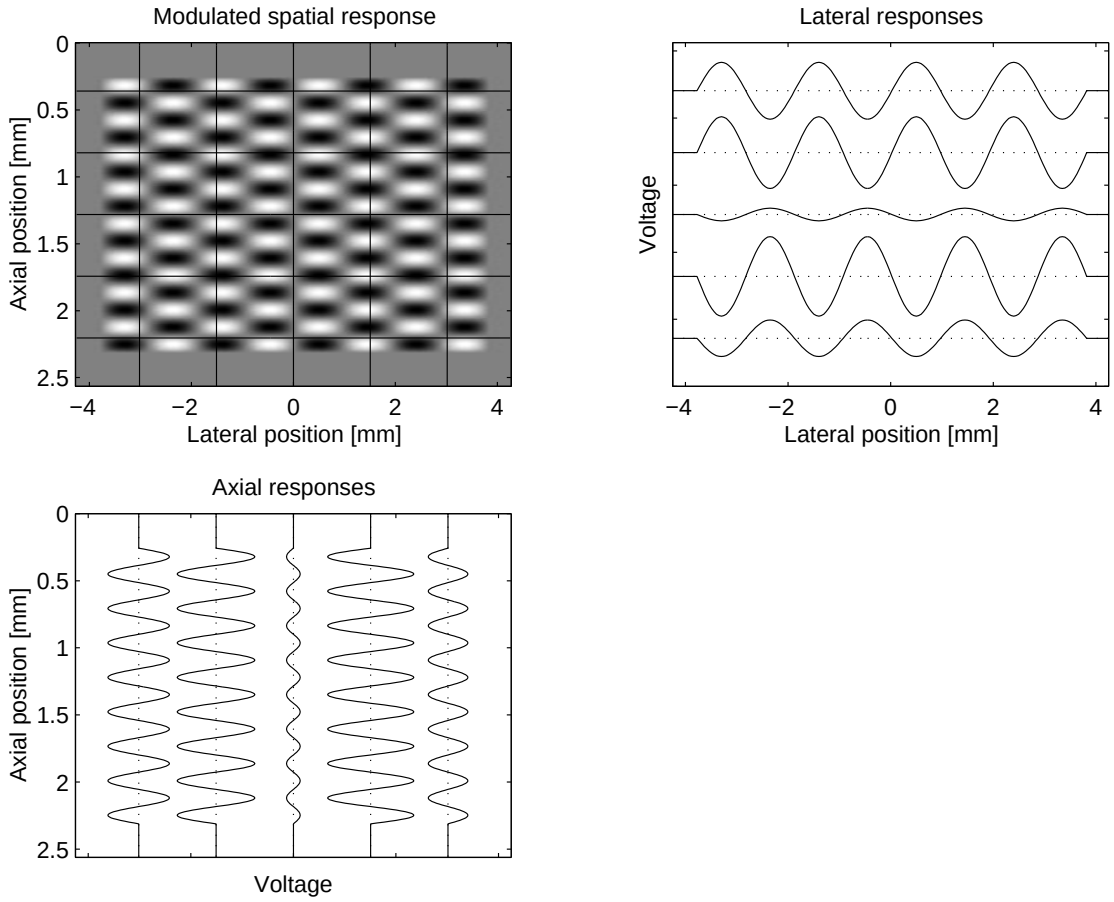

Fig. 3. Received voltage from a single scatterer as a function of spatial position from a field that is modulated in the lateral direction.

system for finding the axial velocity. Such an estimator is described in Section IV.

The lateral modulation can be generated in a multitude of ways. It can be done through the emitted field or from processing the received signals in the receive beamformer. It also can be made by a combination of transmit and receive beamforming. The most flexibility is afforded by mainly making the lateral modulation in the receive processing, because it then can be dynamically adapted to a long range of depths. The reception processing also makes it possible to employ the method in passive sonar, where the sound is received directly from the observed object.

The generation of the lateral modulation can be obtained both from apodization of the transducer array elements and from the phasing of the beam. An example of how such fields can be constructed is given in Section III.

A number of measurements must be obtained for estimating the velocity. For two-dimensional velocity estimation, the samples for the axial velocity are, in the implementation described in this paper, obtained using the traditional method by acquiring the in-phase and quadrature samples. The transverse velocity component is obtained from measurements using two laterally oscillating fields that are 90 degrees phase-shifted relative to each other in the lateral direction, thereby obtaining a spatial quadrature sampling. The use of quadrature beams enables the measurement of the magnitude as well as the sign of the transverse velocity component.

A possible set-up for two-dimensional velocity estimation is presented in Fig. 5. An emit beamformer generates a field suitable for both axial and lateral velocity estimation. Three beamformers are then used for generating the received signals for estimating the axial and lateral velocities. The first beamformer (c) performs conventional focused beamforming for estimating the axial velocity using phase shift estimation. The two other beamformers (a) and (b) focus their beams to generate the in-phase and quadrature signals for the lateral velocity estimation. One set of measurements results from these two beams for each pulse emission. The samples from the axial and lateral beams are fed into the estimator to yield the velocity vector.

III. Field Generation

The transverse spatial oscillation of the field can be generated in a multitude of ways. Different strategies can be applied, and the choice mainly is determined by the number of oscillations needed in the lateral direction. The lateral modulation of the field can be generated by a single array transducer using special beamforming during transmit and/or receive. According to linear system theory, the

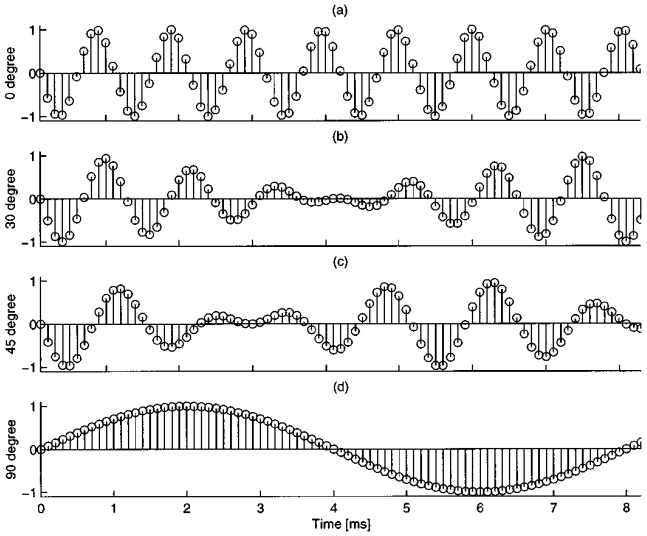

Fig. 4. Received sampled signal for different axial and lateral velocities: (a) $\vec{v} = (v, 0)$, (b) $\vec{v} = (\cos 30°, \sin 30°)v$, (c) $\vec{v} = (\cos 45°, \sin 45°)v$, (d) $\vec{v} = (0, v)$. The velocity magnitude v is 0.25 m/s, f_{prf} is 10 kHz, the transducer center frequency is 3 MHz, and d_x is 2 mm.

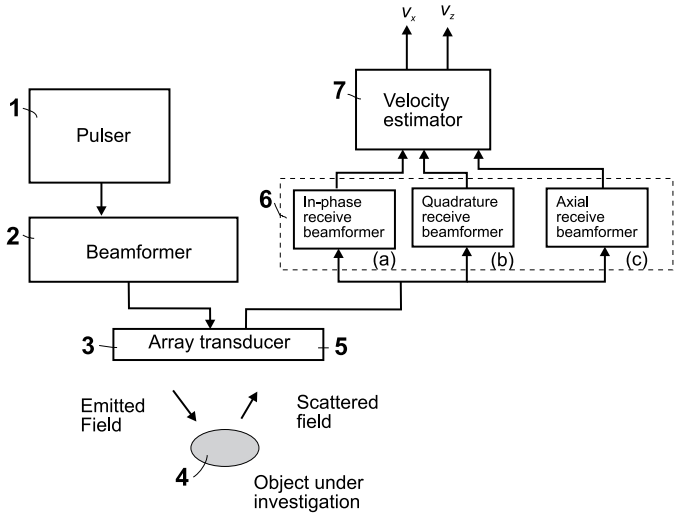

Fig. 5. Block diagram of the main components of the system.

transmit and receive beamforming can be interchanged to generate the resulting field with similar lateral modulation at a certain depth.

The lateral modulation can be generated through apodization or through steering parts of the beams, so that they interact and generate the lateral modulation, or it can be a combination of the two. Apodization functions control the vibration amplitude of the different array elements. Many apodization schemes will lead to a transversely oscillating field, the use of functions with two separate peaks across the aperture being a typical example. The beam steering can be done either as plane-wave interaction or as other forms of focusing at or near the depth for measuring the velocity vector.

A starting point for developing the lateral modulation is to use the theory for continuous wave (CW) fields. Here the radial pressure field variation in the far field region is given by the Fourier transform of the emitting aperture function [15]. Thus, it is possible to give a direct prediction of possible aperture functions.

In designing the measurement situation, it must be noted that the combined field characteristics depend on both the transmitted field and the processing of the received signal. For the far field approximation, where there is no radial phase variation due to diffraction, the pulse-echo radiation pattern can be found by multiplying the transmit pattern with the receive sensitivity pattern.

A. Transmit Apodization Function

Traditional velocity estimation systems uses focusing of the emitted field, and this pulsed field will change shape as a function of depth. This change is not taken into consideration when the velocity component in the radial direction is calculated. To have a spatially oscillating field, which only depends on the applied receive beamforming, nondiffracting beams must be generated in transmit. This ensures that the modulation pattern is independent of the depth, and that the velocity components being measured can become spatially uncorrelated.

Nondiffracting beams, thus, must be used in order to generate a laterally modulated field with a constant spatial frequency measured at a straight line across the beam, orthogonal to the direction of propagation. If diffracting beams are used, a constant spatial frequency can be measured along spherical lines of different radii dependent of the depth, as changes in the phase-fronts of the pulse then are avoided during propagation. Such phase changes will affect the estimator as will curved phase fronts because the lateral frequency is changed through the field for a curved phase front.

Nondiffracting beams exist only in theory for infinitely large apertures as can be seen from a solution to the linear wave equation [16]. In practice the beams of interest are only diffraction-free for a limited range because of the finite aperture used [17]. It has been shown [18], that the fields generated by axicon transducers are similar to the nondiffracting beams proposed by Durnin [16]. The axicon focusing, originally presented by McLeod [19], uses a linearly increasing time delay function from the edge to the center of the aperture. From a focusing point of view, the axicon focusing creates phase coherence along a focal line, whereas quadratic focusing has phase coherence at a point in space. Axicon focus also is referred to as conical focus.

In the replica pulse method [20], the diffraction effects for a plane piston are explained intuitively as the result of the edge wave. The edge wave emanates from the abrupt change in surface velocity at the aperture edge and can be avoided by apodizing the aperture. As stated before, the CW pressure far field can be calculated as the spatial Fourier transform of the aperture's velocity function. It is known from signal analysis that the Fourier transform of the Gaussian function is a Gaussian function. This intuitively indicates that the field from a Gaussian apodized

aperture most likely does not change shape in the near field. When the far field is reached, it still maintains the Gaussian shape with decreasing amplitude and increasing main lobe width as the depth increases.

The amplitude of the CW radially-symmetric pressure field for a Gaussian-apodized piston is [21]:

$$p(\rho, z) = A\frac{\sigma(0)}{\sigma(z)} \exp\left(-\frac{\rho^2}{\sigma^2(z)}\right) \tag{4}$$

where

$$\rho = (x^2 + y^2)^{1/2} \tag{5}$$

and

$$\sigma(z) = \frac{\lambda}{\pi\sigma(0)}\sqrt{z^2 + \frac{\pi^2}{\lambda^2}\sigma^4(0)}. \tag{6}$$

The distance from the center axis is ρ, A is a constant of proportionality, λ is the wavelength in the surrounding medium, and $\sigma(0)$ is the half-width of the amplitude profile at the surface of the transducer. The z-axis is in the propagation direction, and x, y are transverse to the beam axis. The beam half-width is defined as the radial distance ρ_e from the center of the disc at which the amplitude drops to $\frac{1}{e}$ of its maximum. The field properties are controlled by $\sigma(z)$; and (6) shows that the maximum value for $p(\rho, z)$ exists for $z = 0$ and that it decays slowly without any oscillations, thus preserving a Gaussian shape at all depths. On the basis of these observations the transmit apodization function is chosen to be Gaussian.

B. Receive Apodization Function

The receive beamforming must be designed to create the lateral spatial modulation. Determining the receive apodization function is somewhat more complicated, and some direct relation between the transducer characteristics and the field pattern is needed. The far-field CW radiation can be calculated by a Fourier transform of the transducer's front-face velocity distribution [15]; this can be employed in a derivation of the needed apodization pattern. The derivation is based on one-dimensional observations. A comparison to a full three-dimensional pulse-echo simulation with the derived field is presented later.

The relation between the front face velocity distribution $r(\xi)$ at the lateral aperture position ξ and the far-field radiated pressure $R(x)$ at the lateral field position x is [15]:

$$R(x) = k_1 \int_{-\infty}^{\infty} r(\xi) \exp\left(-j\frac{2\pi}{\lambda z}x\xi\right) d\xi \tag{7}$$

when using a far-field para-axial approximation. Here λ is the wavelength, z is axial distance to the field point, and k_1 is a constant of proportionality that is neglected during the following derivation. The integral corresponds to a Fourier transform with a scaling of x by $1/(\lambda z)$.

The lateral modulation must contain a number of oscillations and should be bounded to have a finite probing field. The lateral modulation can thus be described by a lateral oscillation multiplied by a rectangular windows as:

$$R(x) = \text{rect}(L)\cos(2\pi f_x x) \tag{8}$$

where x is lateral distance, f_x is spatial frequency in the lateral direction, and rect(L) denotes a rectangular function of width L centered around $x = 0$. The distance between the lateral peaks is $d_x = 1/f_x$, and the width of the field is L. The desired pattern thus consists of two terms that should be generated by the transducer through the front face apodization function.

Let the velocity distribution of the aperture $r(\xi)$ be a convolution of two functions $r_1(\xi)$ and $r_2(\xi)$:

$$r(\xi) = r_1(\xi) * r_2(\xi) \tag{9}$$

then the radiation pattern becomes:

$$R(x) = \mathcal{F}\{r(\xi)\} = \mathcal{F}\{r_1(\xi) * r_2(\xi)\} = R_1(x)R_2(x) \tag{10}$$

when spatial Fourier transformation is denoted $\mathcal{F}$, and $*$ denotes convolution. The Fourier transform of the rectangular function of width L is:

$$r_1(\xi) = \mathcal{F}\{\text{rect}(L)\} = \frac{L}{z\lambda}\frac{\sin\left(\pi\xi\frac{L}{z\lambda}\right)}{\pi\xi\frac{L}{z\lambda}}. \tag{11}$$

A rectangular field, thus, can be obtained with an aperture function of a sinc. The width of the field is determined by the spacing of the zero crossings in the sinc function. The first zero crossing ξ_0 is at:

$$\xi_0 = \frac{z\lambda}{L}. \tag{12}$$

A wide rectangle thus gives a zero close to the peak at $\xi = 0$ in the sinc function.

The Fourier transform of the cosine term is:

$$r_2(\xi) = \frac{1}{2z\lambda}\left[\delta\left(\frac{\xi}{z\lambda} + f_x\right) + \delta\left(\frac{\xi}{z\lambda} - f_x\right)\right] \tag{13}$$

and combining this with (11) gives:

$$r(\xi) = r_1(\xi) * r_2(\xi) = \frac{L}{2z\lambda}\left(\frac{\sin\left(\pi\left(\frac{\xi}{z\lambda} + f_x\right)L\right)}{\pi\left(\frac{\xi}{z\lambda} + f_x\right)L} + \frac{\sin\left(\pi\left(\frac{\xi}{z\lambda} - f_x\right)L\right)}{\pi\left(\frac{\xi}{z\lambda} - f_x\right)L}\right). \tag{14}$$

Thus, to generate a lateral oscillation, the aperture must have a velocity distribution consisting of two sinc functions. This aperture function will give a field symmetric across the acoustic axis of the aperture. The spatial frequency f_x of the lateral modulation is determined by the distance between the peaks of the two sinc functions and is:

$$f_x = \frac{\xi_t}{z\lambda} = \frac{1}{d_x} \tag{15}$$

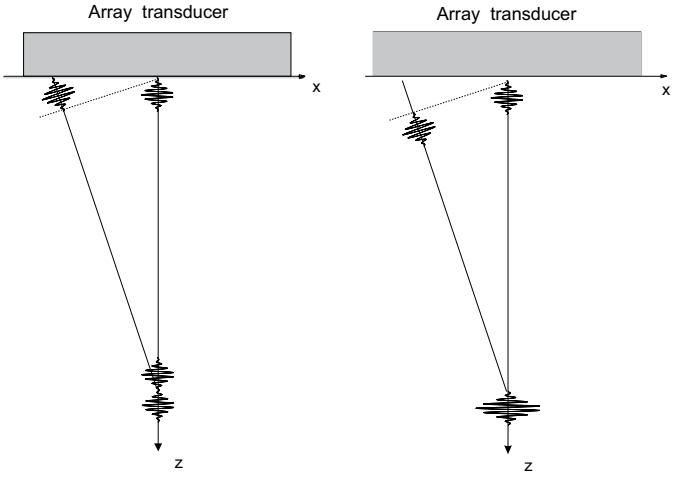

Fig. 6. Alignment of the pulses through delay focusing.

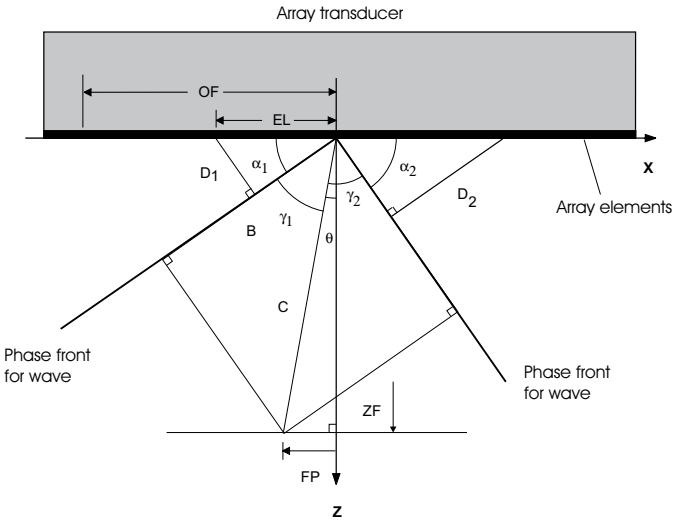

Fig. 7. Definition of geometry for finite plane wave focusing.

where ξ_t is the positive position of the maximum of the sinc function.

The requirement for the velocity estimation is two similar fields phase shifted 90 degrees in relation to each other in the lateral direction. During the receive process, it is possible with an array transducer and a number of beamformers to generate a number of beams in parallel. Both fields, therefore, can be generated in parallel through a simple phasing and apodization before final summation. The two fields can be generated by shifting them by a phase angle θ and $-\theta$, which tilts the beams by $\pm\theta$ from the z-axis [22]. Let a linear phase shift $\exp(jk\theta\xi)$ be added to an aperture apodization $r(\xi)$ by:

$$r_{\text{tilt}}(\xi) = r(\xi)\exp(jk\theta\xi). \tag{16}$$

Here θ is the phase angle and $k = 2\pi/\lambda$ is the wave number.

C. Calculation of Delay Factors

The derivation made above was based on CW theory. Thus, a wave emanating from any point on the aperture can interfere with a wave from any other point on the aperture at any given position in space. The pulse length is in theory infinitely long. In the pulsed mode the pulse length is finite; therefore, the wave fronts must be aligned to interfere at the point of interest. This is illustrated in Fig. 6. For weak focusing this also has the consequence that the relation made in the far field can be found at the focus plane [22].

Conical focusing is used to direct the energy toward the measuring point by aligning the phase fronts for the short pulse used. The two probing beams needed for calculating the lateral velocity component govern the choice of the angles θ, α_1 and α_2 defined in Fig. 7. The cone angles α_1 and α_2 are the angles between the wave fronts and the transducer surface. The position of the center of the oscillating field is controlled by θ.

With reference to Fig. 7, the array element delays are calculated assuming plane wavefronts. The variable OF indicates the center position of the sinc-function with reference to the aperture center, ZF is the depth of interest, EL is the distance from the center of the element to the center of the aperture, and FP indicates the offset of the focal point from the transducer center axis.

The following trigonometric relations are used:

$$\sin\alpha_1 = \frac{D_1}{EL} \tag{17}$$

$$\cos\alpha_1 = \frac{B}{OF} \tag{18}$$

$$\cos\theta = \frac{ZF}{C} \tag{19}$$

$$\sin\theta = \frac{FP}{C} \tag{20}$$

$$\tan\theta = \frac{FP}{ZF} \tag{21}$$

$$\gamma_1 = \frac{\pi}{2} - \alpha_1 - \theta \tag{22}$$

$$\cos\gamma_1 = \frac{B}{C} \tag{23}$$

$$\cos\left(\frac{\pi}{2} - \alpha\right) = \sin\alpha \tag{24}$$

$$\sin(a+b) = \sin a\cos b + \cos a\sin b. \tag{25}$$

Using (18), (20), and (22) in (23) gives:

$$\cos\left(\frac{\pi}{2} - \alpha_1 - \theta\right) = \frac{OF}{FP}\cos\alpha_1\sin\theta \tag{26}$$

and then applying (24) and (25) yields:

$$\cos\alpha_1\sin\theta\left(\frac{OF}{FP} - 1\right) = \sin\alpha_1\cos\theta. \tag{27}$$

Now α_1 can be found using (21)

$$\alpha_1 = \arctan\left(\frac{FP}{ZF}\left(\frac{OF}{FP} - 1\right)\right). \tag{28}$$

The delay in time for the in-phase lateral receive beamforming can be found as

$$D_1 = \frac{1}{c} \cdot EL \cdot \sin\left[\arctan\left(\frac{1}{ZF}\left(OF - |FP|\right)\right)\right] \tag{29}$$

where c is the speed of sound. The delays D_2 for the quadrature lateral receive beamforming are found for a negative value of FP. Thus:

$$D_2 = \frac{1}{c} \cdot EL \cdot \sin\left[\arctan\left(\frac{1}{ZF}\left(OF + |FP|\right)\right)\right]. \tag{30}$$

The focus point FP for beam 1 and 2 must be chosen, so that the radiation patterns are symmetrically placed around the axis. Using the value:

$$FP = \pm\frac{d_x}{8} \tag{31}$$

gives beams that are shifted one quarter of the lateral periode relative to each other, which in turn makes them suitable for the in-phase and quadrature measurements in the lateral direction.

D. Calculation of the Lateral Modulation Frequency

The value to be used for FP can be found from (15) and (31). Because the method used for finding (15) is based on Fraunhofer far-field assumption, two other methods of calculating the lateral wave length using geometric approximations are examined. This is done in order to ensure a proper validation of the lateral wavelength.

First the wavelength is calculated from two plane waves intersecting each other at an angle of 2α with $\alpha = \alpha_1 = \alpha_2$. The second approach uses the intersection of two spherical waves. The actual lateral frequency will be in the range of these two results, since both calculations are approximations to the correct three-dimensional pressure field.

The plane wave interference is shown in Fig. 8. The plane waves are represented by:

$$p_1(t,x,z) = P_1 \exp(-j\omega t) \exp\left(jk\left(xn_x + zn_z\right)\right) \tag{32}$$

and

$$p_2(t,x,z) = P_2 \exp(-j\omega t) \exp\left(jk\left(zn_z - xn_x\right)\right) \tag{33}$$

where P_1 and P_2 are the pressure amplitudes of the waves, and ω is its angular frequency. Here n_x and n_z are the projections of the propagation direction to the respective axis, i.e.:

$$n_x = \sin\alpha$$
$$n_z = \cos\alpha.$$

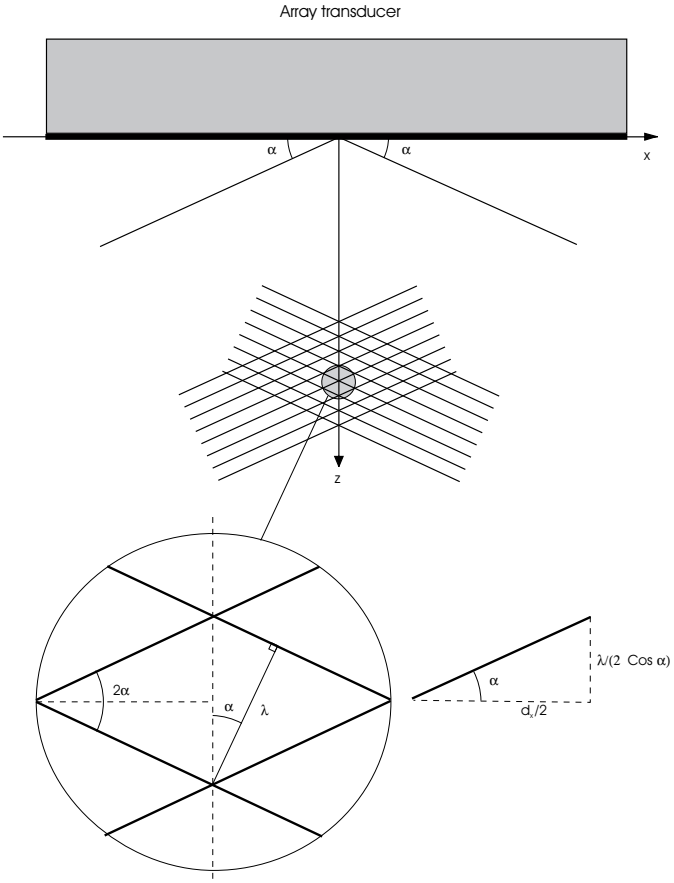

Fig. 8. Intersection of two finite plane waves.

The resulting pressure p_t is, assuming $P_0 = P_1 = P_2$,

$$\begin{aligned} p_t(t,x,z) &= p_1(t,x,z) + p_2(t,x,z) \\ &= P_0 \exp(-j\omega t)\left[\exp\left(jk\left(xn_x + zn_z\right)\right.\right. \\ &\quad \left.\left. + \exp\left(jk\left(zn_z - xn_x\right)\right)\right)\right] \\ &= 2P_0 \exp(-j\omega t) \exp\left(jkzn_z\right) \cos\left(kxn_x\right). \end{aligned} \tag{34}$$

This is a traveling wave in the z direction with an amplitude modulation in the x direction. It must be noted that the resulting wave travels with a phase velocity of:

$$c_{z,\text{phase}} = \frac{c}{n_z}. \tag{35}$$

From the close-up in Fig. 8, the distance between lateral peaks d_x can be found from:

$$\tan\alpha = \frac{\frac{\lambda}{4\cos\alpha}}{\frac{d_x}{4}} \tag{36}$$

yielding

$$d_x = \frac{\lambda}{\sin\alpha}. \tag{37}$$

The longitudinal wave length is:

$$\lambda_z = \frac{\lambda}{\cos\alpha}. \tag{38}$$

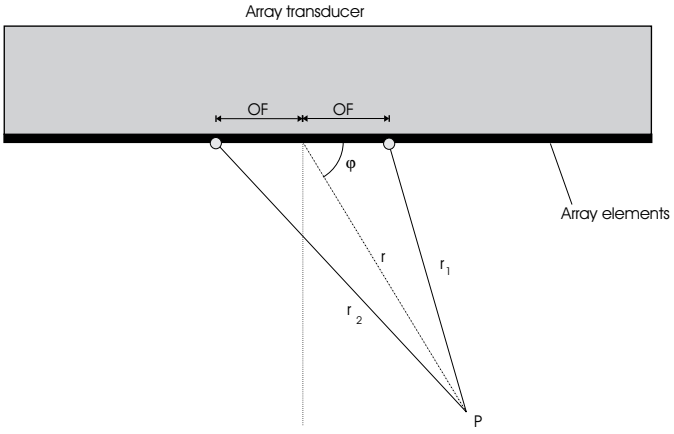

Fig. 9. Geometry for interaction of spherical waves.

Using (28) for $FP = 0$ then:

$$d_x = \frac{\lambda}{\sin\left[\arctan\left(\frac{OF}{ZF}\right)\right]}. \tag{39}$$

Typically $ZF > 2 \cdot OF$ which results in an error of less than 10% using:

$$\sin\left[\arctan\left(\frac{OF}{ZF}\right)\right] \approx \frac{OF}{ZF} \tag{40}$$

which gives a much simpler expression for calculating d_x:

$$d_x = \lambda \frac{ZF}{OF}. \tag{41}$$

This result corresponds to that in (15).

For the derivation using spherical waves, two simple radiators are placed at the centers of the sinc-functions. The geometry is depicted in Fig. 9, and the gray dots indicate the origin for the spherical waves. The pressures of these two spherical waves can be written as:

$$\begin{aligned} p_1(r_1) &= A(r_1)\exp\left(-j\left(\omega t - kr_1\right)\right) \\ p_2(r_2) &= A(r_2)\exp\left(-j\left(\omega t - kr_2\right)\right). \end{aligned} \tag{42}$$

The relation between r, r_1, and r_2 is:

$$\begin{aligned} r_1(r) &= r^2 + OF^2 - 2rOF\cos\varphi \\ r_2(r) &= r^2 + OF^2 + 2rOF\cos\varphi. \end{aligned} \tag{43}$$

The total pressure at a given location r is:

$$\begin{aligned} p_{tot}(r) = A(r_1(r))\exp\left(-j\left(\omega t - kr_1(r)\right)\right) \\ + A(r_2(r))\exp\left(-j\left(\omega t - kr_2(r)\right)\right). \end{aligned} \tag{44}$$

In order to simplify the problem, it is assumed that $r \gg 2OF$, thus:

$$\begin{aligned} r_1 &\approx r - OF\cos\varphi \\ r_2 &\approx r + OF\cos\varphi \end{aligned} \tag{45}$$

and with $A(r) \approx A(r_1) \approx A(r_2)$ the total pressure created by the two interacting spherical waves becomes:

$$\begin{aligned} p_{\mathrm{tot}}(r) &= A(r)\exp(-j\omega t)\cdot \\ &\quad \left[\exp\left(jk\left(r - OF\cos\varphi\right)\right) + \exp\left(jk\left(r + OF\cos\varphi\right)\right)\right] \\ &= A(r)\exp\left(-jk\left(ct - r\right)\right)\cdot \\ &\quad \left[\exp\left(-jkOF\cos\varphi\right) + \exp\left(jkOF\cos\varphi\right)\right] \\ &= 2A(r)\exp\left(-jk\left(ct - r\right)\right)\cos\left(kOF\cos\varphi\right). \end{aligned} \tag{46}$$

The spatial frequency for the radial field is not constant. The width $\Delta\varphi$ of the first lobe for the direction φ is defined by the angles φ_{01} and φ_{02} of the zeros for $\cos(kOF\cos\varphi) = 0$ given by:

$$\begin{aligned} kOF\cos\varphi_{01} &= \frac{\pi}{2} \\ kOF\cos\varphi_{02} &= -\frac{\pi}{2}. \end{aligned} \tag{47}$$

The width is:

$$\Delta\varphi = \left|\varphi_{01} - \varphi_{02}\right|. \tag{48}$$

The radial wavelength λ_r is governed by:

$$\lambda_r/2 = r \cdot \Delta\varphi. \tag{49}$$

When $kOF > 2OF \gg \lambda$ the angles will be very close to $\pi/2$, and this small difference is denoted δ. Hereby:

$$\begin{aligned} \varphi_{01} &= \frac{\pi}{2} - \delta \\ \varphi_{02} &= \frac{\pi}{2} + \delta \\ \left|\varphi_{01} - \varphi_{02}\right| &= 2\delta \end{aligned}$$

and

$$\cos\left(\frac{\pi}{2} - \delta\right) = \sin\delta$$

and

$$\sin\delta \approx \delta \quad \text{for} \quad |\delta| \ll 1$$

then

$$\Delta\varphi = \frac{\pi}{kOF} = \frac{\lambda}{2OF} \tag{50}$$

and the radial wavelength λ_r is given at the depth of interest by:

$$\lambda_r = ZF \cdot \frac{\lambda}{OF}. \tag{51}$$

This result corresponds to that in (41) and (51), showing that the three methods for the stated conditions give approximately the same results. The lateral wavelength is thus determined by the depth, the distance between the sinc peaks, and the fundamental RF frequency of the emitted pulse.

E. Field Simulation Example

Using a nonfocused Gaussian apodization for the transmit beam and two sinc functions for apodization along with axicon plane wave focusing for receive beamforming, results in a field with a sensitivity that oscillates spatially in the transverse direction. The receive beamforming, that generates the lateral modulation by apodization and plane wave focusing can be controlled dynamically by moving the center and the scaling of the sinc function to control the lateral wavelength and the number of oscillations. The advantage of this approach, instead of transmit focusing and apodization, is the ability to obtain a controlled spatially oscillating field for all depths.

The basic principle derived from the above was examined for a pulsed system using the Field simulation program [23]. The form of the transmit field basically should be independent of the depth because a traveling Gaussian plane wave is nondiffracting [21]. A linear array transducer with 64 elements with a width of 0.41 mm, height 5.0 mm, and a pitch[2] of 0.51 mm was used. An 8 cycle, 3 MHz pulse was used in the simulation.

The emitted pressure fields for nonfocused and focused Gaussian apodized transducers are shown in Figs. 10 and 11. The pulsed field is calculated for specific depths to illustrate the evolution of the pulse shape as it travels.

To create a similar illustration of the receive sensitivity in Fig. 12, the setup for the receive beamforming is used in a transmit simulation. Hereby the construction of the lateral oscillation can be illustrated, although this is only created during receive beamforming. The apodization and delay values used are shown in Fig. 13.

The number of zeros from the top of the sinc-function to the edge is 5, and the offset (OF) of the sinc top from the center of the tranducer is 18 times the pitch. The interference of the two waves is clearly seen in Fig. 12.

The resulting pulse-echo sensitivity fields for a depth of 70 mm are shown in Fig. 14 for the in-phase and quadrature channel, respectively. The displacement for the pressure fields of one-fourth of the lateral wavelength can be observed.

For the configuration chosen, d_x is:

$$d_x = \lambda \frac{ZF}{OF} = \frac{1540}{3 \cdot 10^6} \frac{70}{18 \cdot 0.51} = 3.9 \cdot 10^{-3} \qquad [\mathrm{m}]\,.$$

The distance found by inspection of the actual generated acoustical field was 4 mm (Fig. 15), which is in very good agreement with the predicted value.

The sinc is calculated to have a zero at a fictional element adjacent to the edge element in order to reduce edge waves to a minimum. The number of zeros from the top of the sinc to the edge of the aperture determines the bandwidth of the transversal oscillation. Truncating the sinc corresponds to multiplication with a rectangular window. The effect on the field is a convolution of the ideal field with the Fourier transform of the window.

[2]The pitch is the distance from the center of one element to the center of the adjacent element.

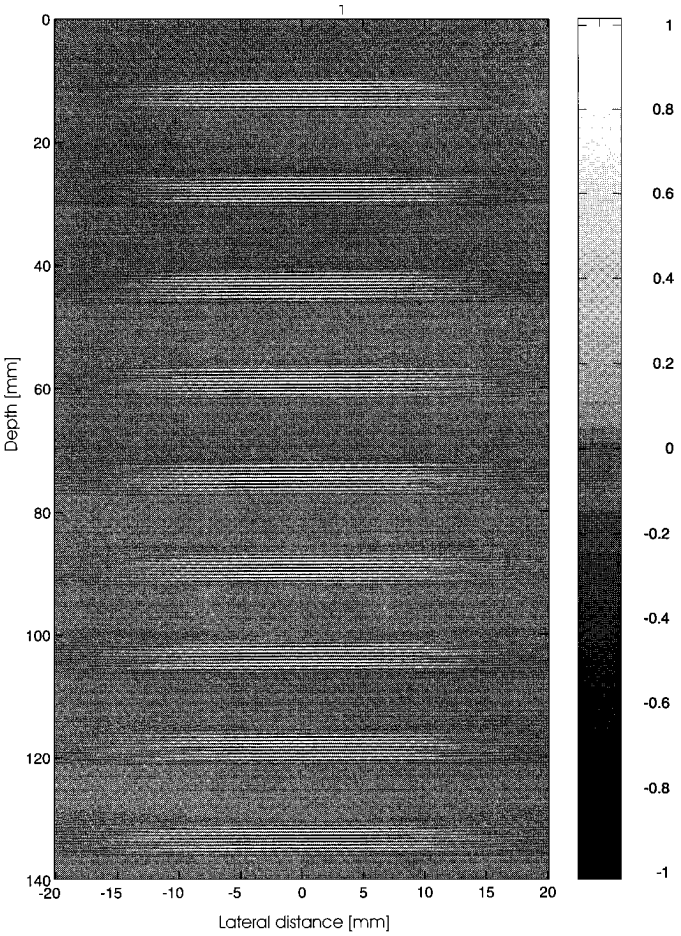

Fig. 10. Emitted pressure field for unfocused Gaussian beam as a function of depth.

To display the lateral wavelength, the envelope of the axial direction is calculated for an emitted pressure field. The envelope is calculated using the Hilbert transform of the time signal. The lateral modulation at one point in time in the middle of the pulse field are shown in Fig. 16. The result is calculated for different numbers of zeros (number of zeros = 3, 5, 7) in the sinc apodization function. This demonstrates the effect of the width of the sinc function on the lateral field oscillation. A narrower main lobe (more zeros) in the sinc function results in more oscillations with a higher amplitude in the lateral field. This shows that a lateral modulation suitable for transverse velocity estimation can be generated, which was the central goal here. A broad, nondiffracting emit field was used, and the lateral modulation was solely created through receive focusing and apodization. This yields a fairly broad lateral field, but this should not be seen as a central limiting factor for the approach. An emit focusing can be introduced to narrow the probing field and make d_x smaller, and this is the topic of further research. More information about the field generation can be found in [14].

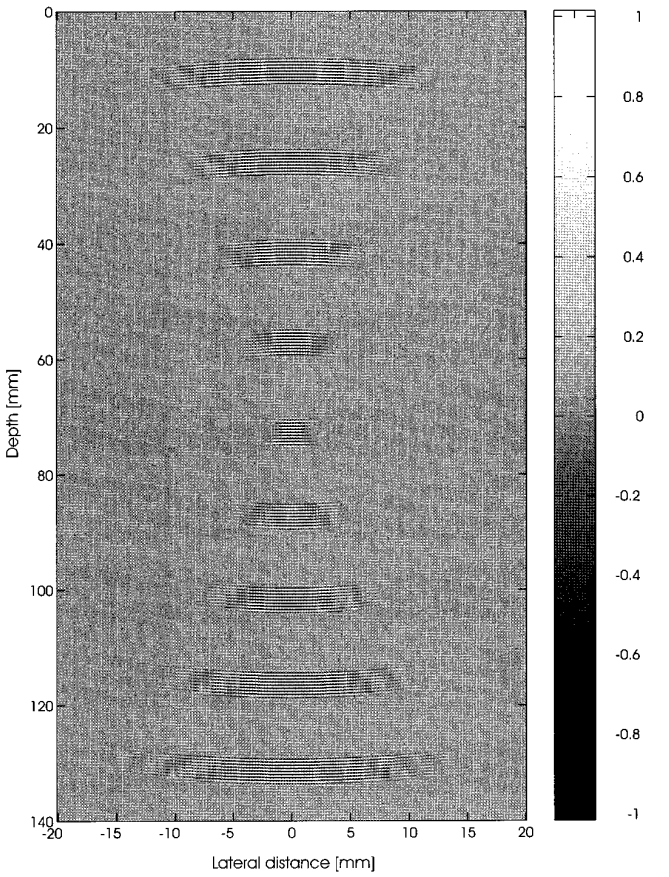

Fig. 11. Emitted pressure field for focused Gaussian beam as a function of depth.

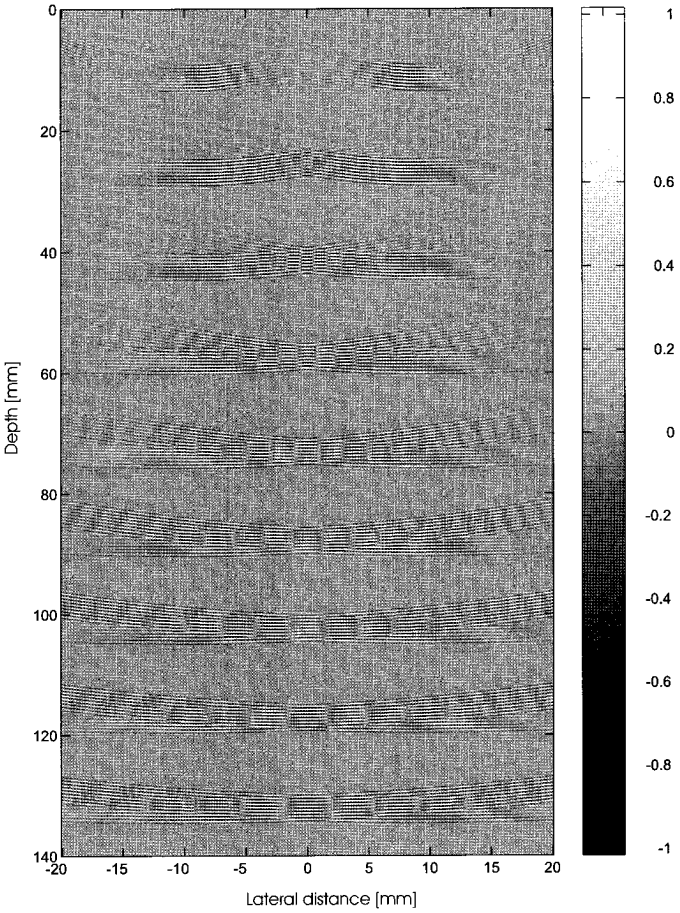

Fig. 12. Emitted pressure field for two interacting finite plane waves used for creating a transverse modulation.

IV. Estimation Algorithm

The estimator must determine both the axial and lateral velocity. A compensation for the axial velocity must be done before determining the lateral velocity. Therefore, the axial velocity is determined first.

The signal from the axial beamformer is passed on to the axial velocity processor, which samples the signal at the time $t = 2d/c$, where d is the depth in tissue and c is the speed of sound. A second quadrature sample is acquired at time $t = 2d/c + 1/(4f_0)$, where f_0 is the center frequency of the emitted pulse. One set of samples is taken for each pulsed field received, and the samples for line number i are denoted $x(i)$ and $y(i)$. The first signal has the number $i = 0$. The axial velocity is found by using the equation [1], [3]:

$$v_z = -\frac{c}{4\pi T_{prf} f_0} \times \arctan\left(\frac{\sum_{i=0}^{N_c-2} y(i+1)x(i) - x(i+1)y(i)}{\sum_{i=0}^{N_c-2} x(i+1)x(i) + y(i+1)y(i)}\right) \quad (52)$$

where T_{prf} is the time between pulse emissions from the array, and N_c is the number of pulse-echo lines in the same direction used in the estimator.

The axial velocity is used for selecting the samples from the left and right signals from the two other beamformers.

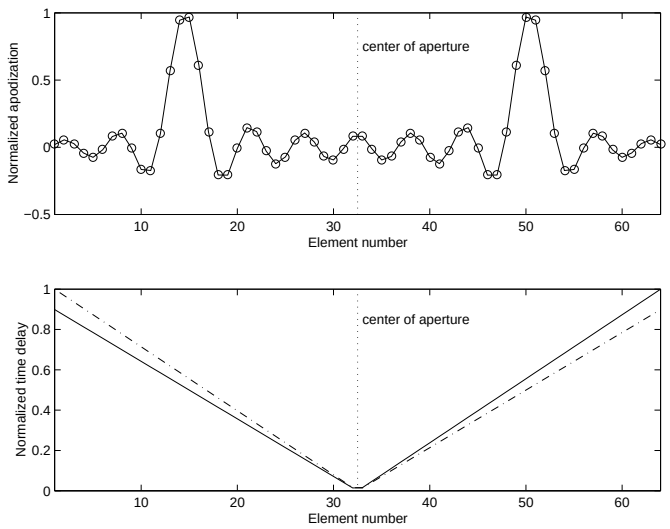

Fig. 13. Time delay and amplitude apodization values used on the individual transducer elements for creating the lateral modulation during receive beamforming.

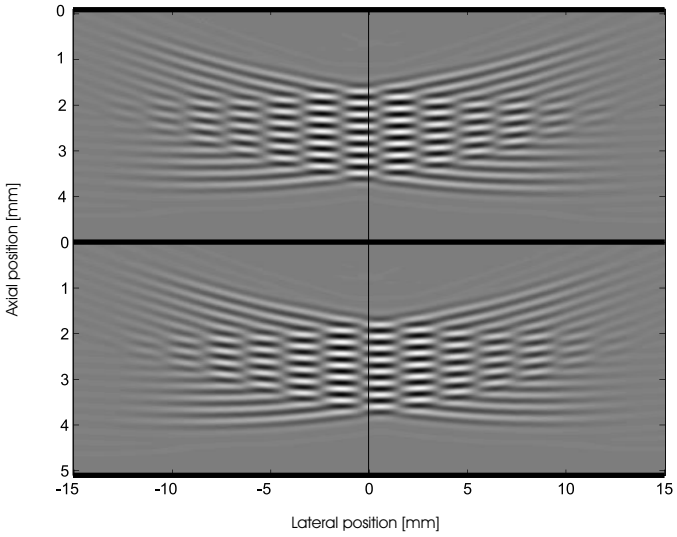

Fig. 14. Received voltage for a single scatterer as a function of its position at a depth of 70 mm. The in-phase voltage is shown on the top and the quadrature voltage is shown on the bottom.

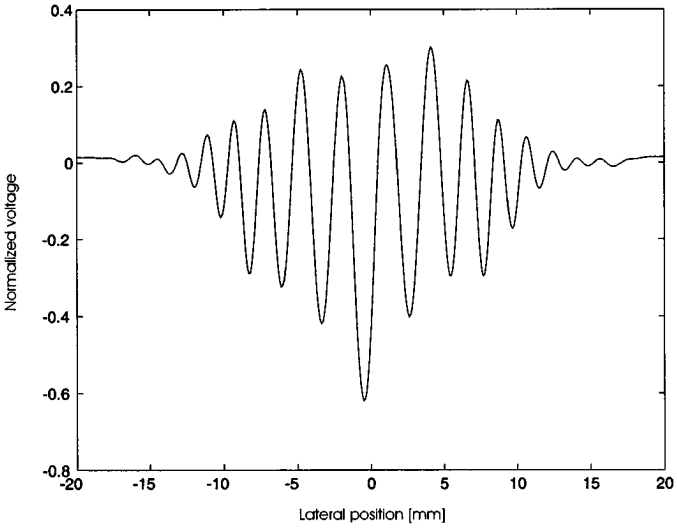

Fig. 15. Voltage response as a function of lateral position for the pulsed field used in the example.

The samples taken from the left signals, denoted $g_l(t)$, are given by:

$$x_l(i) = g_l\left(\frac{2d}{c} - \frac{2v_z T_{prf}}{c} i\right) \tag{53}$$

so as to compensate for the influence from the axial movement of the blood. Correspondingly, samples taken from the right signals, denoted $g_r(t)$, is given by:

$$y_r(i) = g_r\left(\frac{2d}{c} - \frac{2v_z T_{prf}}{c} i\right). \tag{54}$$

These samples enter the estimator given by:

$$v_x = -\frac{c}{2\pi T_{prf} f_x} \times \arctan\left(\frac{\sum_{i=0}^{N_c-2} y_r(i+1)x_l(i) - x_l(i+1)y_r(i)}{\sum_{i=0}^{N_c-2} x_l(i+1)x_l(i) + y_r(i+1)y_r(i)}\right) \tag{55}$$

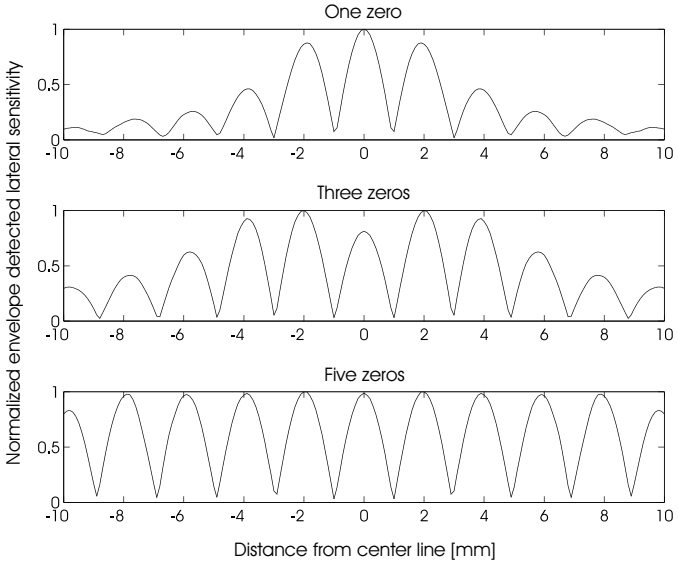

Fig. 16. Lateral response with oscillations as a function of zeros in the sinc apodization function.

where f_x is the frequency of the laterally oscillating transducer field at the particular depth. Then v_x is the transverse velocity.

V. Performance

The functionality of the method is examined for two-dimensional velocity vector measurement and is documented by simulations. The simulation is performed using the impulse response method developed by Tupholme [24] and by Stepanishen [25] in the implementation developed by Jensen and Svendsen [23]. The high accuracy of this approach, when compared to measurements, is described in Jensen [26]. The paper showed that the simulated pressure values were within 1% of the measured ultrasound fields. The simulation approach is applicable for pulsed fields and is used for three-dimensional modeling of the response from a collection of scatterers.

The simulated situation is shown in Fig. 17. A vessel of 10 mm diameter is placed 70 mm from the center of the transducer array, i.e., on the axis of the transducer. The vessel contains plug flow (all blood scatterers have the same velocity), and the 15,000 scatterers in the vessel have a Gaussian scattering amplitude distribution with zero mean value and unit variance. This ensures fully developed speckle in the response from the blood model. The simulation is done for constant velocity of 1 m/s and a varying angle (θ) for the flow vector. The angles used are 0, 15, 35, 55, 75, and 90 degrees. The estimator uses 50 RF lines for finding an estimate and the experiment has been repeated 20 times for each angle. The 64-element array transducer specified in Section III-D was used during the simulation.

Fig. 5 shows the implementation of the method applied here for the measurement of blood velocity in two dimen-

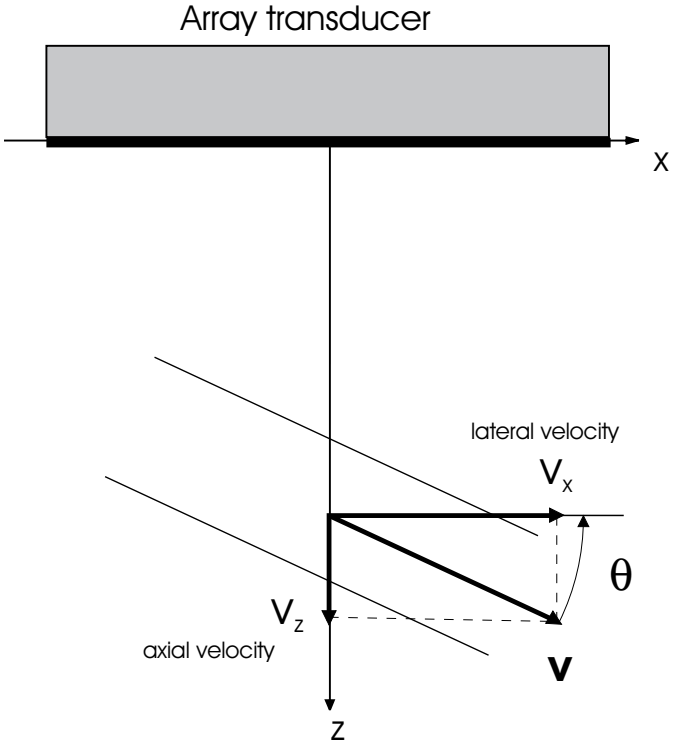

Fig. 17. Definition of axial and lateral velocity for the computer experiment.

sions. It consists of a generator or pulser, 1; an emit beam former, 2; a linear array ultrasound emitting transducer, 3; a linear array ultrasound receiving transducer, 5; three receive beam formers, 6a, 6b, and 6c working in parallel and receiving signals from the receiving transducer. The beamformed signals are fed into the estimator, 7; that calculates the velocity vector. The pulser, 1, generates a pulsed voltage signal with a number of sinusoidal oscillations at a frequency of f_0 in each pulse, that is used in the emit beam former, 2. The emit beam former, 2, is capable of individually attenuating and delaying the signals to each of the elements of the transducer array, 3. In this simulation no delay is introduced during emission, and in Fig. 18 the attenuation values are shown as a function of element number in the transducer. This is done to emit a broad field that can be used for forming all three beams in parallel. A linear array transducer is used for both emitting and receiving the pulsed ultrasound field. The emitted field from the transducer is scattered by the blood in the blood vessel, and part of the scattered field is received by the linear array transducer. The signals from the individual elements are passed on to two of the receive beam formers, i.e., 6a and 6b in Fig. 5. The signals from the elements are individually scaled in amplitude and individually delayed and are finally summed to yield a single output signal from each receive beamformer. The first receive beamformer, 6a in Fig. 5, generates the left signal and the second receive beamformer, 6b in Fig. 5, generates the right signal. Fig. 13 shows both the delay values and the corresponding amplitude scaling factors for both receive beamformers.

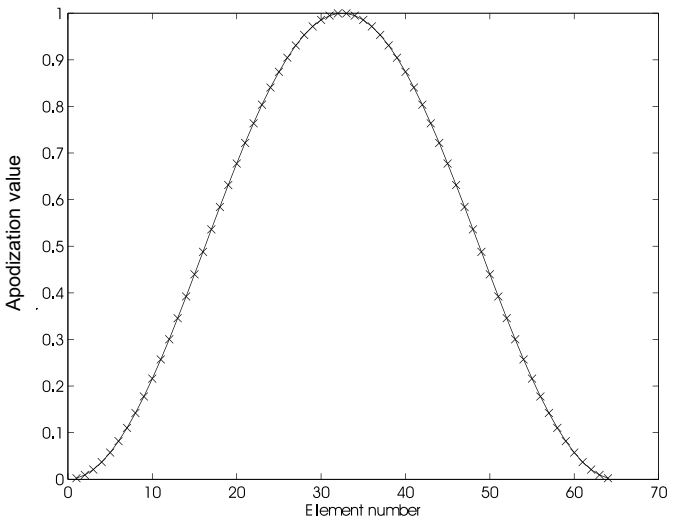

Fig. 18. Amplitude scaling factors or equivalently, apodization, used for the emit beam former.

The third receive beam former, 6c in Fig. 5, generates the signal for estimating the axial component.

The result of the simulation is shown in Fig. 19. The true velocity vectors are indicated by the small arrows. The gray ellipses for each velocity vector estimate indicate the standard deviations for both the axial estimation and the lateral estimation, respectively. The lateral standard deviation is the semi-major axis, and the axial standard deviation is the semi-minor axis. The mean values of the estimates are illustrated by the circles at the centers of the ellipses. The average performance for all angles is: mean velocity 0.99 m/s, longitudinal S.D. of the estimates 0.015 m/s and lateral S.D. of the estimates 0.196 m/s. For flow parallel to the transducer the results are: mean velocity 0.95 m/s, angle 0.1°, longitudinal S.D. 0.020 m/s, and lateral S.D. 0.172 m/s.

The velocity estimation has only been done at a fixed distance from the transducer in the simulation. Due to the use of a nonfocused field, it is possible to dynamically change the focusing of the three receive beam formers to generate the spatially oscillating field at other depths for the same emitted field, as was demonstrated in Section III.

The example described here only estimated the velocity in a plane, but the method can be changed to give the full three-dimensional velocity vector. A two-dimensional matrix transducer must then be used as described by Smith *et al.* [27]. The same emission field can be used because it is unfocused. An extra set of receive beam formers must then be employed to make the velocity estimation in the y-direction perpendicular to both the z- and x-directions.

VI. Summary

A new method for velocity vector estimation has been presented. It uses a single array transducer for measuring the axial and transverse velocity, which makes it conve-

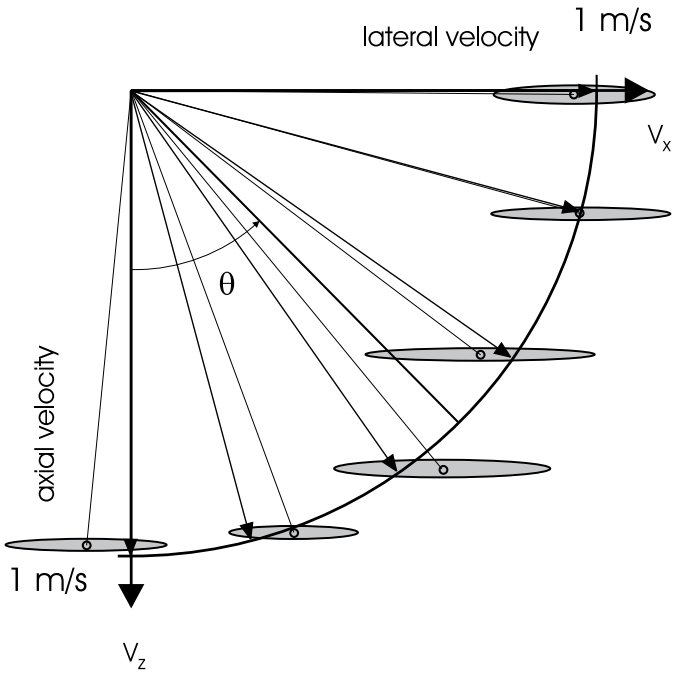

Fig. 19. Resulting standard deviations for the estimated mean velocities. The true velocity vectors are indicated by the small arrows. The gray ellipses for each velocity vector estimate indicate the standard deviations for both the axial estimation and the lateral estimation, respectively. The lateral standard deviation is the semi-major axis, and the axial standard deviation is the semi-minor axis. The mean values of the estimates are illustrated by the circles at the centers of the ellipses.

nient to use a small aperture window. The axial and lateral velocities are estimated, and the sign of the lateral velocity is determined by using two receive beamformers.

The method uses a number of consecutive pulse emissions and compares the received signals to minimize the effects from media dependent distortions like attenuation and refraction. The method thus only uses the difference from pulse to pulse to determine the velocity.

Only two measurements are taken from each beam for determining the lateral velocity, so that a very modest amount of calculations must be performed to estimate the transverse velocity. Employing a standard autocorrelation approach makes the method robust in terms of noise in the measurement process, since this estimator is unbiased for white noise.

The method can be expanded to find the full velocity vector by using a third beam former, then all the components of the three-dimensional velocity vector can be estimated.

Acknowledgments

The authors would like to thank Søren Kragh Jespersen, Paul F. Stetson, Jens E. Wilhjelm, and Ole Trier Andersen, all at the Department of Information Technology, who struggled through the many versions of this paper, found errors, and came up with numerous improvements.

References

[1] J. A. Jensen, *Estimation of Blood Velocities Using Ultrasound: A Signal Processing Approach*. New York: Cambridge Univ. Press, 1996.

[2] D. W. Baker, "Pulsed ultrasonic Doppler blood-flow sensing," *IEEE Trans. Sonics Ultrason.*, vol. SU-17, pp. 170–185, 1970.

[3] C. Kasai, K. Namekawa, A. Koyano, and R. Omoto, "Real-time two-dimensional blood flow imaging using an autocorrelation technique," *IEEE Trans. Sonics Ultrason.*, vol. 32, pp. 458–463, 1985.

[4] K. Namekawa, C. Kasai, M. Tsukamoto, and A. Koyano, "Realtime bloodflow imaging system utilizing autocorrelation techniques," in *Ultrasound '82*, R. A Lerski and P. Morley, Eds., New York: Pergamon Press, 1982, pp. 203–208.

[5] D. Dotti, E. Gatti, V. Svelto, A. Uggè, and P. Vidali, "Blood flow measurements by ultrasound correlation techniques," *Energia Nuclear*, vol. 23, pp. 571–575, 1976.

[6] O. Bonnefous, P. Pesqué, and X. Bernard, "A new velocity estimator for color flow mapping," *Proc. IEEE Ultrason. Symp.*, 1986, pp. 855–860.

[7] M. I. Skolnik, *Introduction to Radar Systems*. New York: McGraw-Hill, 1980.

[8] G. E. Trahey, J. W. Allison, and O. T. von Ramm, "Angle independent ultrasonic detection of blood flow," *IEEE Trans. Biomed. Eng.*, vol. BME-34, pp. 965–967, 1987.

[9] J. A. Jensen, "Artifacts in velocity estimation using ultrasound and cross-correlation," *Med. Biol. Eng. Comp.*, vol. 32/4, Suppl., pp. s165–s170, 1994a.

[10] M. D. Fox, "Multiple crossed-beam ultrasound Doppler velocimetry," *IEEE Trans. Sonics Ultrason.*, vol. SU-25, pp. 281–286, 1978.

[11] H. F. Routh, T. L. Pusateri, and D. D. Waters, "Preliminary studies into high velocity transverse blood flow measurement," *Proc. IEEE Ultrason. Symp.*, 1990, pp. 1523–1526.

[12] V. L. Newhouse, D. Censor, T. Vontz, J. A. Cisneros, and B. B. Goldberg, "Ultrasound Doppler probing of flows transverse with respect to beam axis," *IEEE Trans. Biomed. Eng.*, vol. BME-34, pp. 779–788, 1987.

[13] P. A. Magnin, "Doppler effect: History and theory," *Hewlett-Packard J.*, vol. 37, pp. 26–31, 1986.

[14] P. Munk, "Estimation of the 2-D flow vector in ultrasonic imaging: a new approach," M.S. thesis, Dept. Information Technology, Technical University of Denmark, Lyngby, Denmark, 1996.

[15] J. W. Goodman, *Introduction to Fourier Optics*, 2nd ed. New York: McGraw Hill, 1996.

[16] J. Durnin, "Exact solutions for non-diffracting beams. I: the scalar theory," *J. Opt. Soc. Amer.*, vol. 4, pp. 651–654, 1987.

[17] J. Durnin and J. J. J. Miceli, "Diffraction-free beams," *Amer. Phys. Soc. J.*, vol. 58, pp. 1499–1501, 1987.

[18] J. A. Campbell, "Generation of a nondiffracting beam with frequency independent beamwidth," *J. Acoust. Soc. Amer.*, vol. 88, pp. 2467–2477, 1990.

[19] J. H. McLeod, "The axicon: A new type of optical element," *J. Opt. Soc. Amer.*, vol. 44, pp. 592–597, 1954.

[20] A. Freedman, "Acoustic field of a pulsed circular piston," *J. Sound Vibration*, vol. 170, pp. 495–519, 1994.

[21] D. K. Hsu, F. J. Margetan, M. D. Hasselbusch, S. J. Wormley, H. S. Hughes, and D. O. Thompson, "Technique for nonuniform poling of piezoelectric element and fabrication of gaussian transducers," *IEEE Trans. Ultrason., Ferroelect., Freq. Contr.*, vol. 37, pp. 404–410, 1990.

[22] B. D. Steinberg, *Principles of Aperture and Array System Design*. New York: Wiley, 1976.

[23] J. A. Jensen and N. B. Svendsen, "Calculation of pressure fields from arbitrarily shaped, apodized, and excited ultrasound transducers," *IEEE Trans. Ultrason., Ferroelect., Freq. Contr.*, vol. 39, pp. 262–267, 1992.

[24] G. E. Tupholme, "Generation of acoustic pulses by baffled plane pistons," *Mathematika*, vol. 16, pp. 209–224, 1969.

[25] P. R. Stepanishen, "Transient radiation from pistons in an infinte planar baffle," *J. Acoust. Soc. Amer.*, vol. 49, pp. 1629–1638, 1971.

[26] J. A. Jensen, "A model for the propagation and scattering of ultrasound in tissue," *J. Acoust. Soc. Amer.*, vol. 89, pp. 182–191, 1991a.

[27] S. W. Smith, H. G. Pavy, and O. T. von Ramm, "High-speed ultrasound volumetric imaging system—Part I: Transducer design and beam steering," *IEEE Trans. Ultrason., Ferroelect., Freq. Contr.*, vol. 38, pp. 100–108, 1991.

Jørgen Arendt Jensen (M'93) received his M.S. degree in electrical engineering in 1985 and the Ph.D. degree in 1989, both from the Technical University of Denmark. He received the Dr.Techn. from the university in 1996.

Dr. Jensen has published a number of papers on signal processing and medical ultrasound and the book *Estimation of Blood Velocities Using Ultrasound*, Cambridge University Press in 1996. He has been a visiting scientist at Duke University, Stanford University, and the University of Illinois at Urbana-Champaign. He is currently full professor of Biomedical Signal Processing at the Technical University of Denmark at the Department of Information Technology.

Peter Munk was born in Grenaa, Denmark, 1963. He received the Bachelor of Engineering degree (electrical) in 1987 and his M.Sc. degree in 1996 from the Technical University of Denmark (DTU). He currently is a Ph.D. candidate at the Department of Information Technology, DTU.

His research interests are in acoustics and signal processing (space-time and time-frequency) for application within ultrasound imaging and flow measurements.